On the use of dispersion analysis for model assessment in structural identification

Vasileios K Dertimanis

Abstract

One of the most important issues faced in parametric time-domain identification and subsequent experimental/operational modal analysis is the correct estimation of model order, which in turn determines the number of structural vibration modes. The aim of this study is to provide a quantitative and physically meaningful framework for model order assessment that is characterized by global applicability, in the sense of implementation in both state-space and transfer function model representations. To this end and under the assumption of stationary wideband excitation, a novel dispersion analysis scheme is proposed for the quantification of every mode's relative importance to the total stochastic response, which is based on a modal decomposition of the covariance matrix. Subsequently, after defining the modal dispersion matrix, a corresponding metric is introduced and used either as a stand alone tool for model order assessment, or as an extension of existing tools, such as stabilization diagrams. The method is validated through both simulated (NASA Mini-Mast truss) and experimental (suspended steel subframe flexible structure) identification problems, for which a subspace and a prediction-error estimation method are utilized and compared under the proposed quantitative indices. Moreover, performance comparisons with other energy-based metrics are also reported. The results indicate that the proposed method can be effectively used in parametric time-domain structural identification, for both order assessment and comparison of diverse model-based estimation methods.

1. Introduction

Modern engineering structures are amenable to a wide and diverse variety of design objectives. These include not only the standard low cost and maximum safety demands, but also the compliance to environmentally induced specifications emerging from systematic approaches, such as life-cycle design and design for environment. These requirements call for the establishment of smart interactions with the structure throughout its service life, for monitoring, state assessment, and proactive management.

The process of identifying discrete-time models from multichannel excitation and response (or response only) measurements clearly falls within the aforementioned framework. Indeed, time-series analysis (Lütkepohl, 2005; Box et al., 2008) and system identification (Ljung, 1999) have shown to be effective and valuable tools that retain crucial technological importance in the fields of data-driven modeling (Papakos and Fassois, 2003; Andersen, 1997; Koulocheris et al., 2008; Bayraktar et al., 2011), control (Landau and Zito, 2006; De Korte, 2009) and structural health monitoring (Farrar and Worden, 2006; Farrar and Lieven, 2007; Dertimanis and Koulocheris, 2008; Morassi and Vestroni, 2008). This is why the implementation of corresponding techniques to structural systems

Department of Civil Engineering and Geomatics, Cyprus University of Technology, Cyprus

Received: 12 July 2013; accepted: 15 July 2013

Corresponding author:
Vasileios K Dertimanis, Department of Civil Engineering and Geomatics, Faculty of Engineering and Technology, Cyprus University of Technology, P.O. Box 5032, Limassol 3603, Cyprus.
Email: vasileios.dertimanis@cut.ac.cy

(airplanes, bridges, oil platforms, vehicles, buildings, etc.), where the human and environmental safety factors are of primary concern, has gained increased attention and remains a very active engineering research area (Ren and Zong, 2004; Antonacci et al., 2012; Dertimanis et al., 2012; Loh et al., 2013).

One of the most important issues in parametric time-domain structural identification is the choice of model order, which controls the number of estimated vibration modes for subsequent experimental/operational modal analysis (Larbi and Lardies, 2000; Reynders, 2012). This parameter corresponds to the size of the state vector, when state-space models (internal descriptions) are employed (Katayama, 2005; Verhaegen and Verdult, 2007), or to the order of the (vector) autoregressive (AR) polynomial, when transfer function models (external descriptions) are considered (Ljung, 1999, Chapter 4). Naturally, the interrelation between the internal and the external descriptions (Hannan, 1976; Yang et al., 1994) implies a straightforward dependence between the size of the state vector and the order of the AR polynomial (Lardies, 2008; Dertimanis and Koulocheris, 2009).

Regarding model order assessment and corresponding estimation of structural vibration modes, a wide majority of reported application studies (Bayraktar et al., 2011; Caicedo, 2011; Antonacci et al., 2012) rely heavily on the use of frequency stabilization diagrams. Apart from the fact that the latter have a clear *nonparametric* setting, they are amenable to a number of reported inconsistencies that include sensitivity to noise, frequency slitting, and stabilization of spurious modes. The use of clearing tools (Van Der Auweraer and Peeters, 2004) for the better visual interpretation of stabilization diagrams is a significant step forward, especially in respect to automated operation modal analysis (Reynders et al., 2012), yet the inherent nonparametric nature and other fundamental discrepancies (especially the stabilization of spurious modes) may still be present. However, it must be pointed out that frequency stabilization diagrams comprise one *global* measure of model order assessment, in the sense that they are applicable to all time-domain parametric identification methods and to all model representations.

In addition, there is a very limited number of tools that distinguish structural from extraneous modes, which, in general, are method-specific. Within the context of the Eigensystem Realization Algorithm (ERA) (Juang and Pappa, 1985), application of the modal amplitude coherence has been reported to be problematic in certain cases (Florakis et al., 2001). Dispersion analysis (Lee and Fassois, 1993; Lee and Lee, 2001) has provided significant indications of effectiveness (Papakos and Fassois, 2003), yet, it has been developed for use only in transfer function model representations, while its residue-based calculation (Fassois, 2001) may be prone to numerical issues. Recently introduced schemes that are based on model reduction, as the one developed by Goethals and De Moor (2002) and extended by Reynders and De Roeck (2008) to the modal transfer norm metric, provide a measure of the error when an associated mode is removed from the model. These latter schemes seem effective and they can be attributed as global, since they can be easily applied to both state-space and transfer function model representations, through the transformation of the latter to the former, which is a numerically efficient process. They are however indirect and do not estimate the actual amount of stochastic vibration energy contributed by a specific mode.

This study develops a novel model order assessment tool through the generalization of the notion of modal dispersion, as the latter has been introduced by Lee and Fassois (1993). Taking into account the effectiveness of this metric to the order validation of transfer function representations (Petsounis and Fassois, 2001), it is extended to cover state-space models as well, obtaining thus a *global* attribute. Using the spectral factorization of the state matrix and the properties of the corresponding spectral projectors, a modal decomposition of the output covariance matrix is introduced and subsequently applied to the definition of a modal dispersion matrix. It is then shown how this matrix can be utilized towards the quantitative assessment of the contribution that every vibration mode retains in the total structural response, under the assumption of stochastic wideband excitation. Moreover, in an inverse framework, the same quantitative assessment is applied to the estimation of structural degrees of freedom and to the distinction of structural from spurious modes. The proposed framework is validated through the structural identification problem of a suspended steel subframe flexible structure, in both output-only (operational modal analysis) and input–output (experimental modal analysis) identification.

The contributions of this study are (a) the introduction of a covariance modal decomposition in closed form that can be used to indirectly validate a model through comparisons with nonparametric covariance estimates, (b) the introduction of a *modal dispersion matrix* (MDM) and its associated *modal dispersion norm* (MDN) that quantifies the contribution of each structural mode to the total vibration energy, under stochastic broadband excitation, (c) the implementation of MDN as a *global* model order assessment tool in parametric time-domain identification, and (d) the utilization of MDN in conjunction to frequency stabilization diagrams for the detection of spurious modes.

The rest of the paper is organized as follows: Section 2 covers the dispersion analysis and the

definition of MDM. Its application to structural identification, including the definition of MDNs is treated in Section 3. Section 4 contains the identification experiments, and in Section 5 the conclusions are drawn, along with some further remarks and suggestions for future research.

2. Dispersion analysis of structural systems

2.1. Preliminaries

The equation of motion for a linear, viscously damped structural system with n degrees-of-freedom is

$$\mathbf{M} \cdot \ddot{\mathbf{q}}(t) + \mathbf{D} \cdot \dot{\mathbf{q}}(t) + \mathbf{K} \cdot \mathbf{q}(t) = \mathbf{P} \cdot \mathbf{f}(t) \tag{1}$$

where $\mathbf{M}$, $\mathbf{D}$ and $\mathbf{K}$ are the real (and possibly symmetric) $[n \times n]$ mass, viscous damping and stiffness matrices, $\mathbf{q}(t)$ is the $[n \times 1]$ vibration displacement vector, $\mathbf{f}(t)$ is the $[p \times 1]$ vector of excitations and $\mathbf{P}$ is a $[n \times p]$ "coordinates" matrix. By defining a $[2n \times 1]$ state vector as $\mathbf{x}(t) = [\mathbf{q}^T \ \dot{\mathbf{q}}^T]^T$, a corresponding state-space realization of equation (1) is formulated as ($\mathbf{M}$ is assumed full rank)

$$\dot{\mathbf{x}}(t) = \mathbf{A}_c \cdot \mathbf{x}(t) + \mathbf{B}_c \cdot \mathbf{f}(t) \tag{2a}$$

$$\mathbf{y}(t) = \mathbf{C}_c \cdot \mathbf{x}(t) + \mathbf{D}_c \cdot \mathbf{f}(t) \tag{2b}$$

with the matrices of the state equation (2a) being defined as

$$\mathbf{A}_c = \begin{bmatrix} \mathbf{O}_n & \mathbf{I}_n \\ -\mathbf{M}^{-1} \cdot \mathbf{K} & -\mathbf{M}^{-1} \cdot \mathbf{D} \end{bmatrix} [2n \times 2n],$$

$$\mathbf{B}_c = \begin{bmatrix} \mathbf{0} \\ \mathbf{M}^{-1} \cdot \mathbf{P} \end{bmatrix} [2n \times p] \tag{3}$$

and the matrices of the output equation (2b) being dependent to the type of $\mathbf{y}(t)$

$$\mathbf{y}(t) = \mathbf{q}(t) \ (\text{displacement}):$$
$$\mathbf{C}_c = \begin{bmatrix} \mathbf{I}_n & \mathbf{O}_n \end{bmatrix} [n \times 2n], \quad \mathbf{D}_c = \mathbf{0} \tag{4a}$$

$$\mathbf{y}(t) = \dot{\mathbf{q}}(t) \ (\text{velocity}):$$
$$\mathbf{C}_c = \begin{bmatrix} \mathbf{O}_n & \mathbf{I}_n \end{bmatrix} [n \times 2n], \quad \mathbf{D}_c = \mathbf{0} \tag{4b}$$

$$\mathbf{y}(t) = \ddot{\mathbf{q}}(t) \ (\text{acceleration}):$$
$$\mathbf{C}_c = \begin{bmatrix} -\mathbf{M}^{-1} \cdot \mathbf{K} & -\mathbf{M}^{-1} \cdot \mathbf{D} \end{bmatrix} [n \times 2n], \quad \mathbf{D}_c = \mathbf{M}^{-1} \cdot \mathbf{P} \tag{4c}$$

Under the zero-order-hold (ZOH) principle, which assumes constant intersample behavior of the excitation

vector signal (Fadali, 2009, Section 7.6), the discrete-time equivalent of the system described by equation (2) is

$$\mathbf{x}[t + 1] = \mathbf{A}_d \cdot \mathbf{x}[t] + \mathbf{B}_d \cdot \mathbf{f}[t] \tag{5a}$$

$$\mathbf{y}[t] = \mathbf{C}_d \cdot \mathbf{x}[t] + \mathbf{D}_d \cdot \mathbf{f}[t] \tag{5b}$$

with $\mathbf{C}_d = \mathbf{C}_c$, $\mathbf{D}_d = \mathbf{D}_c$ and

$$\mathbf{A}_d = e^{\mathbf{A}_c \cdot T_s}, \quad \mathbf{B}_d = [\mathbf{A}_d - \mathbf{I}] \cdot \mathbf{A}_c^{-1} \cdot \mathbf{B}_c \tag{6}$$

where T_s (s) denotes the sampling period.

2.2. The displacement/velocity case

When $\mathbf{D}_d = 0$ the discrete-time state-space equation takes the form

$$\mathbf{x}[t + 1] = \mathbf{A}_d \cdot \mathbf{x}[t] + \mathbf{B}_d \cdot \mathbf{f}[t] \tag{7a}$$

$$\mathbf{y}[t] = \mathbf{C}_d \cdot \mathbf{x}[t] \tag{7b}$$

For the subsequent definition of modal dispersion, the following result is fundamental.

Lemma 2.1: *Consider the state-space model of equation (7) and let the excitation be uncorrelated and stationary. Then, a decomposition of the covariance matrix of the output time-series $\mathbf{y}[t]$ is*

$$\mathbf{\Gamma}_{yy}[h] \equiv E\{\mathbf{y}[t + h] \cdot \mathbf{y}^T[t]\} = \sum_{k=1}^{2 \cdot n} \mathbf{Q}_k \cdot \lambda_k^h \tag{8}$$

where h is the time lag, $\mathbf{Q}_k$ is defined in the following proof, and λ_k is the kth eigenvalue of the state matrix $\mathbf{A}_d$.

Proof: Let $\mathbf{f}[t]$ be a zero-mean stationary process with covariance matrix

$$\mathbf{\Gamma}_{ff}[h] = \mathbf{\Sigma}_{ff} \cdot \delta[h] \tag{9}$$

where $\delta[h]$ denotes Kronecker's delta. Let also the spectral decomposition of the state matrix be given by (Meyer, 2000, pp. 520, 526)

$$f(\mathbf{A}_d) = \sum_{k=1}^{2 \cdot n} \mathbf{G}_k \cdot f(\lambda_k) \tag{10}$$

with f denoting a function that is defined for every λ_k and $\mathbf{G}_k$ the spectral projectors (for which $\mathbf{G}_k^2 = \mathbf{G}_k$, $\mathbf{G}_i \cdot \mathbf{G}_j = \mathbf{O}$, for $i \neq j$ and $\sum_k \mathbf{G}_k = \mathbf{I}$). The state

equation can be written as an infinite moving average process of the form

$$\mathbf{x}[t] = \sum_{k=0}^{\infty} \mathbf{A}_d^k \cdot \mathbf{B}_d \cdot \mathbf{f}[t - k - 1] \qquad (11)$$

The covariance matrix of the process described by equation (11) is (Brockwell and Davis, 2002, p. 244)

$$\mathbf{\Gamma}_{xx}[h] \equiv E\{\mathbf{x}[t + h] \cdot \mathbf{x}^{\mathrm{T}}[t]\} = \sum_{j=0}^{\infty} \mathbf{A}_d^{j+h} \cdot \mathbf{\Sigma} \cdot [\mathbf{A}_d^j]^{\mathrm{T}} \quad (12)$$

for $h = 0, \pm 1, \pm 2, \ldots$, where $\mathbf{\Sigma} = \mathbf{B}_d \cdot \mathbf{\Sigma}_{ff} \cdot \mathbf{B}_d^{\mathrm{T}}$. Substitution of equation (10) with equation (12) implies

$$\mathbf{\Gamma}_{xx}[h] = \sum_{j=0}^{\infty} \left\{ \sum_{k=1}^{2 \cdot n} \mathbf{G}_k \cdot \lambda_k^{j+h} \cdot \mathbf{\Sigma} \cdot \sum_{m=1}^{2 \cdot n} \mathbf{G}_m^{\mathrm{T}} \cdot \lambda_m^j \right\} \qquad (13)$$

The last expression can be manipulated as follows

$$\mathbf{\Gamma}_{xx}[h] = \sum_{k} \sum_{m} \mathbf{G}_k \cdot \mathbf{\Sigma} \cdot \mathbf{G}_m^{\mathrm{T}} \cdot \lambda_k^h \cdot \sum_{j=0}^{\infty} \lambda_k^j \cdot \lambda_m^j$$

$$= \sum_{k} \sum_{m} \mathbf{G}_k \cdot \mathbf{\Sigma} \cdot \mathbf{G}_m^{\mathrm{T}} \cdot \lambda_k^h \cdot \frac{1}{1 - \lambda_k \cdot \lambda_m}$$

$$= \sum_{k=1}^{2 \cdot n} \mathbf{G}_k \cdot \mathbf{\Sigma} \sum_{m=1}^{2 \cdot n} \frac{\mathbf{G}_m^{\mathrm{T}}}{1 - \lambda_k \cdot \lambda_m} \cdot \lambda_k^h \qquad (14)$$

Setting,

$$\mathbf{P}_k = \mathbf{G}_k \cdot \mathbf{\Sigma} \cdot \sum_{m=1}^{2 \cdot n} \frac{\mathbf{G}_m^{\mathrm{T}}}{1 - \lambda_k \cdot \lambda_m} \qquad (15)$$

leads to

$$\mathbf{\Gamma}_{xx}[h] = \sum_{k=1}^{2 \cdot n} \mathbf{P}_k \cdot \lambda_k^h \qquad (16)$$

Then, since, from equation (7b), $\mathbf{\Gamma}_{yy}[h] = \mathbf{C}_d \cdot \mathbf{\Gamma}_{xx}[h] \cdot \mathbf{C}_d^{\mathrm{T}}$, the result of equation (8) follows immediately, with $\mathbf{Q}_k = \mathbf{C}_d \cdot \mathbf{P}_k \cdot \mathbf{C}_d^{\mathrm{T}}$. Υ

Remark 1: Towards the proof of Lemma 2.1 the discrete-time Lyapunov equation can be applied instead (Kailath et al., 2000, p. 267). The aforementioned proof is, however, more closely related to a times-series analysis framework.

Remark 2: Clearly, equation (8) is a *modal decomposition*. If the eigenvalues of the state matrix appear in complex conjugate pairs (refer to Dertimanis and Koulocheris (2011) when real modes are also present), then

$$\mathbf{\Gamma}_{yy}[h] = \sum_{k=1}^{n} \mathbf{Q}_k \cdot \lambda_k^h + \mathbf{Q}_k^* \cdot (\lambda_k^*)^h \qquad (17)$$

where the asterisk denotes a complex conjugate (in the case of matrices the operator applies to every entry). Equation (17) is henceforth referred to as the *output covariance matrix modal decomposition* (CMMD). In the same way, the expansion of equation (16) into n terms, just as in equation (17), reveals the state CMMD. A similar modal decomposition has been reported by (Reynders, 2012, p. 74). See also Dertimanis and Koulocheris (2011) and Dertimanis and Koulocheris (2009).

Remark 3: The zero-lag output CMMD is given by

$$\mathbf{\Gamma}_{yy}[0] = \sum_{k=1}^{n} \mathbf{Q}_k + \mathbf{Q}_k^* \qquad (18)$$

and it can be used to the evaluation of the total vibration energy associated with the output of the state-space realization, under stochastic wideband excitation. To this end, the following definitions are given.

Definition 2.2: *The kth modal dispersion matrix is defined as*

$$\mathbf{E}_k = \mathbf{Q}_k + \mathbf{Q}_k^* \qquad (19)$$

and it can be used to assess the contribution of the kth mode to the total stochastic vibration energy.

Definition 2.3: *The kth normalized modal dispersion matrix is defined as the matrix with elements*

$$[\Delta_k]_{ij} = \frac{[\mathbf{E}_k]_{ij}}{[\sum_{m=1}^{n} \mathbf{E}_m]_{ij}} \cdot 100\% = \frac{[\mathbf{E}_k]_{ij}}{[\mathbf{\Gamma}_{yy}[0]]_{ij}} \cdot 100\% \quad (20)$$

and it can be used to assess the relative contribution of the kth mode to the total stochastic vibration energy.

From equation (18) it follows that every modal dispersion matrix includes both autocovariance and cross-covariance terms. Regarding the latter, in certain cases the off-diagonal elements may appear negative, which implies that the corresponding modal impulse response acts in a way that opposes the total vibration response, reducing thus its magnitude (Lee and Fassois, 1993; Lee and Lee, 2001).

2.3. The acceleration case

For acceleration output the direct transmission term is added to the output equation of the state-space model:

$$\mathbf{x}[t+1] = \mathbf{A}_d \cdot \mathbf{x}[t] + \mathbf{B}_d \cdot \mathbf{f}[t] \tag{21a}$$

$$\mathbf{y}[t] = \mathbf{C}_d \cdot \mathbf{x}[t] + \mathbf{D}_d \cdot \mathbf{f}[t] \tag{21b}$$

The covariance matrix associated with equation (21b) is

$$\boldsymbol{\Gamma}_{yy}[h] = \mathbf{C}_d \cdot \boldsymbol{\Gamma}_{xx}[h] \cdot \mathbf{C}_d^{\mathrm{T}} + \mathbf{C}_d \cdot \boldsymbol{\Gamma}_{xf}[h] \cdot \mathbf{D}_d^{\mathrm{T}}$$
$$+ \mathbf{D}_d \cdot \boldsymbol{\Gamma}_{fx}[h] \cdot \mathbf{C}_d^{\mathrm{T}} + \mathbf{D}_d \cdot \boldsymbol{\Gamma}_{ff}[h] \cdot \mathbf{D}_d^{\mathrm{T}} \tag{22}$$

where the cross-covariance matrices are defined in a similar way to that shown in the first part of equation (12). The existence of the three trailing terms in the right–hand side prevents equation (22) from obtaining the modal decomposition form of equation (8) for all lags. Instead, corresponding expressions may be derived by employing the discrete-time Lyapunov equation (Kailath et al., 2000, p. 267). Alternatively, it is easy to show that

$$\boldsymbol{\Gamma}_{xf}[h] \equiv E\{\mathbf{x}[t+h] \cdot \mathbf{f}^{\mathrm{T}}[t]\}$$
$$= \begin{cases} \mathbf{A}_d^{h-1} \cdot \mathbf{B}_d \cdot \boldsymbol{\Sigma}_{ff} & h = 1, 2, 3, \ldots \\ \mathbf{O} & \text{otherwise} \end{cases} \tag{23}$$

by utilizing equation (11). Indeed

$$\boldsymbol{\Gamma}_{xf}[h] = \sum_{k=0}^{\infty} \mathbf{A}_d^k \cdot \mathbf{B}_d \cdot E\{\mathbf{f}[t+h-k-1] \cdot \mathbf{f}^{\mathrm{T}}[t]\}$$
$$= \sum_{k=0}^{\infty} \mathbf{A}_d^k \cdot \mathbf{B}_d \cdot \boldsymbol{\Sigma}_{ff} \cdot \delta[h-k-1]$$
$$= \mathbf{B}_d \cdot \boldsymbol{\Sigma}_{ff} \cdot \delta[h-1] + \mathbf{A}_d \cdot \mathbf{B}_d \cdot \boldsymbol{\Sigma}_{ff} \cdot \delta[h-2]$$
$$+ \mathbf{A}_d^2 \cdot \mathbf{B}_d \cdot \boldsymbol{\Sigma}_{ff} \cdot \delta[h-3] + \cdots$$

from which equation (23) follows naturally. Similarly,

$$\boldsymbol{\Gamma}_{fx}[h] \equiv E\{\mathbf{f}[t+h] \cdot \mathbf{x}^{\mathrm{T}}[t]\}$$
$$= \begin{cases} \boldsymbol{\Sigma}_{ff} \cdot \mathbf{B}_d^{\mathrm{T}} \cdot [\mathbf{A}_d^{h+1}]^{\mathrm{T}} & h = -1, -2, -3, \ldots \\ \mathbf{O} & \text{otherwise} \end{cases} \tag{24}$$

In this respect, equation (22) becomes

$$\boldsymbol{\Gamma}_{yy}[h] = \mathbf{C}_d \cdot \boldsymbol{\Gamma}_{xx}[h] \cdot \mathbf{C}_d^{\mathrm{T}}$$
$$+ \begin{cases} \mathbf{C}_d \cdot \mathbf{A}_d^{h-1} \cdot \mathbf{B}_d \cdot \boldsymbol{\Sigma}_{ff} \cdot \mathbf{D}_d^{\mathrm{T}} & h = 1, 2, 3, \ldots \\ \mathbf{D}_d \cdot \boldsymbol{\Sigma}_{ff} \cdot \mathbf{D}_d^{\mathrm{T}} & h = 0 \\ \mathbf{D}_d \cdot \boldsymbol{\Sigma}_{ff} \cdot \mathbf{B}_d^{\mathrm{T}} \cdot [\mathbf{A}_d^{h+1}]^{\mathrm{T}} \cdot \mathbf{C}_d^{\mathrm{T}} & h = -1, -2, -3, \ldots \end{cases} \tag{25}$$

so corresponding modal decompositions can be extracted. For example, that for positive-lag is derived by observing that

$$\mathbf{C}_d \cdot \mathbf{A}_d^{h-1} \cdot \mathbf{B}_d \cdot \boldsymbol{\Sigma}_{ff} \cdot \mathbf{D}_d^{\mathrm{T}} = \sum_{k=1}^{2 \cdot n} \frac{\mathbf{C}_d \cdot \mathbf{G}_k \cdot \mathbf{B}_d \cdot \boldsymbol{\Sigma}_{ff} \cdot \mathbf{D}_d^{\mathrm{T}}}{\lambda_k} \cdot \lambda_k^h \tag{26}$$

where the spectral theorem of the state matrix (equation (10)) was again employed. Then the positive-lag $\boldsymbol{\Gamma}_{yy}[h]$ is also described by equation (8), with $\mathbf{Q}_k$ replaced by $\mathbf{Q}_k^+$ and

$$\mathbf{Q}_k^+ = \mathbf{C}_d \cdot \mathbf{G}_k \cdot \mathbf{B}_d \cdot \boldsymbol{\Sigma}_{ff} \cdot \left[\sum_{k=1}^{2 \cdot n} \frac{(\mathbf{C}_d \cdot \mathbf{G}_m \cdot \mathbf{B}_d)^{\mathrm{T}}}{1 - \lambda_k \cdot \lambda_m} + \frac{\mathbf{D}_d^{\mathrm{T}}}{\lambda_k} \right] \tag{27}$$

In order to derive $\boldsymbol{\Gamma}_{yy}[0]$ and the associated modal dispersion expressions for the acceleration case, a decomposition of the direct transmission term is required. It can be found in (Reynders, 2012, p. 73) that $\mathbf{D}_d = \mathbf{C}_d \cdot (\mathbf{A}_d - \mathbf{I})^{-1} \cdot \mathbf{B}_d$ (under the ZOH assumption). Since

$$(\mathbf{A}_d - \mathbf{I})^{-1} = -\sum_{k=1}^{2 \cdot n} \frac{\mathbf{G}_k}{1 - \lambda_k} \tag{28}$$

it follows that

$$\mathbf{D}_d \cdot \boldsymbol{\Sigma}_{ff} \cdot \mathbf{D}_d^{\mathrm{T}}$$
$$= \mathbf{C}_d \cdot \sum_{k=1}^{2 \cdot n} \frac{\mathbf{G}_k}{1 - \lambda_k} \cdot \mathbf{B}_d \cdot \boldsymbol{\Sigma}_{ff} \cdot \mathbf{B}_d^{\mathrm{T}} \cdot \sum_{m=1}^{2 \cdot n} \frac{\mathbf{G}_m^{\mathrm{T}}}{1 - \lambda_m} \cdot \mathbf{C}_d^{\mathrm{T}}$$
$$= \mathbf{C}_d \cdot \sum_{k=1}^{2 \cdot n} \mathbf{G}_k \boldsymbol{\Sigma} \cdot \sum_{m=1}^{2 \cdot n} \frac{\mathbf{G}_m^{\mathrm{T}}}{(1 - \lambda_k) \cdot (1 - \lambda_m)} \cdot \mathbf{C}_d^{\mathrm{T}} \tag{29}$$

Combining equations (16), (25) and (29), the zero-lag covariance matrix for the acceleration case complies with equation (8) as well, with $\mathbf{Q}_k$ replaced by $\mathbf{Q}_k^0$ and

$$\mathbf{Q}_k^0 = \mathbf{C}_d \cdot \mathbf{G}_k \cdot \boldsymbol{\Sigma} \cdot \sum_{m=1}^{2 \cdot n} \frac{(1 - \lambda_k) + (1 - \lambda_m)}{(1 - \lambda_k \cdot \lambda_m) \cdot (1 - \lambda_k) \cdot (1 - \lambda_m)}$$
$$\cdot (\mathbf{C}_d \cdot \mathbf{G}_m)^{\mathrm{T}} \tag{30}$$

Obviously, the remarks and the definitions of the previous section apply to the acceleration case with no modifications, except the expressions of equations (27), (30).

3. Application to system identification

The basic results of the previous section can be integrated into the structural identification problem, if they are considered in an inverse setting. More specifically, given an estimated model in state-space form, dispersion analysis can be used to assess its order and to detect the presence of spurious modes. In this respect, the following metrics can be employed.

Definition 3.1: *The L_2 and L_∞ modal dispersion metrics are defined as the corresponding matrix norms of the associated modal dispersion matrix*

$$\delta_{E,k,2} = \|\mathbf{E}_k\|_2 \quad \text{or} \quad \delta_{\Delta,k,2} = \|\Delta_k\|_2 \tag{31a}$$

$$\delta_{E,k,\infty} = \|\mathbf{E}_k\|_\infty \quad \text{or} \quad \delta_{\Delta,k,\infty} = \|\Delta_k\|_\infty \tag{31b}$$

where $k = 1, 2, \ldots, n$. Moreover, a normalized dispersion metric is a number between 0 and 1 defined as

$$\bar{\delta}_{\natural,k,\#} = \frac{\delta_{\natural,k,\#}}{\max\limits_{k}(\delta_{\natural,k,\#})} \tag{32}$$

for $\natural = E, \Delta$ and $\# = 2, \infty$. Each one of the quantities defined above can be attributed to a specific mode. The latter can be thus characterized by one additional quantity that accompanies the natural frequency, the damping ratio, and the mode shape. This can be proved extremely conveniently during the validation of a parametric model. For example, a dispersion metric can be used to find out whether a spurious mode (characterized by negligible contribution to the total vibration energy) appears as structural in a stabilization diagram (see Section 4).

Apart from the dispersion metrics, the covariance expression of equation (8) and the CMMDs of equation (17) can be implemented in the validation of candidate models, either by visualizing the contribution of an individual mode, or through comparisons to sample covariance matrix estimates.

3.1. Transfer function model representations

The result of a parametric identification process is a description of the monitored system in state-space or transfer function format. In its general form, the latter usually arrives as (Ljung, 1999),

$$\mathbf{y}[t] = \mathbf{K}(q) \cdot \mathbf{f}[t] + \mathbf{L}(q) \cdot \mathbf{e}[t] \tag{33}$$

with $\mathbf{K}(q)$ and $\mathbf{L}(q)$ denoting multivariate transfer functions that describe the output-to-input and the output-to-noise dynamics, respectively, q as backshift operator, $q^{-k} \cdot \mathbf{y}[t] = \mathbf{y}[t-k]$, and $\mathbf{e}[t]$ as a multivariate zero mean white noise process. Equation (33) shows that the output can be expressed as $\mathbf{y}[t] = \mathbf{y}_s[t] + \mathbf{y}_n[t]$, where $\mathbf{y}_s[t]$ and $\mathbf{y}_n[t]$ are obviously defined and refer to the system and noise dynamics, respectively. Focusing on the former and since $\mathbf{K}(q)$ can be factorized as a product of two matrix polynomials of order np, $\mathbf{y}_s[t]$ can be written in a recursive way as (Box et al., 2008)

$$\mathbf{y}_s[t] + \sum_{i=1}^{np} \mathbf{V}_i \cdot \mathbf{y}[t-i] = \mathbf{W}_0 \cdot \mathbf{f}[t] + \sum_{j=1}^{np} \mathbf{W}_j \cdot \mathbf{f}[t-j] \tag{34}$$

where the $\mathbf{V}_i$'s and $\mathbf{W}_j$'s are matrices of appropriate sizes. Then, a straightforward state-space realization in the form of equation (21) can be achieved by selecting the following states (Juang and Pappa, 1985; Yang et al., 1994)

$$\mathbf{x}_i[t] = \mathbf{x}_{i+1}[t-1] + \mathbf{b}_i \cdot \mathbf{f}[t-1], \quad i = 1, 2, \ldots, np-1 \tag{35a}$$

$$\mathbf{x}_p[t] = -\sum_{j=1}^{np-1} \mathbf{x}_j[t-1] + \mathbf{b}_p \cdot \mathbf{f}[t-1] \tag{35b}$$

with $\mathbf{b}_i = \mathbf{W}_i + \sum_{j=0}^{i-1} \mathbf{V}_{i-j} \cdot \mathbf{b}_j$ and $\mathbf{b}_0 = \mathbf{W}_0$, after which the associated matrices become

$$\mathbf{A}_d = \begin{bmatrix} \mathbf{O} & \mathbf{I} & \cdots & \mathbf{O} \\ \mathbf{O} & \mathbf{O} & \cdots & \mathbf{O} \\ \vdots & \vdots & \ddots & \vdots \\ \mathbf{O} & \mathbf{O} & \cdots & \mathbf{I} \\ -\mathbf{V}_{np} & -\mathbf{V}_{np-1} & \cdots & -\mathbf{V}_1 \end{bmatrix},$$

$$\mathbf{B}_d = \begin{bmatrix} \mathbf{b}_1 \\ \mathbf{b}_2 \\ \vdots \\ \mathbf{b}_{np-1} \\ \mathbf{b}_{np} \end{bmatrix}, \quad \mathbf{C}_d = [\mathbf{I} \ \mathbf{O} \ \cdots \ \mathbf{O}], \quad \mathbf{D}_d = \mathbf{W}_0 \tag{36}$$

In the above setting only the $\mathbf{b}_i$'s need to be calculated in order to formulate the state-space model. Note also that the utilized realization is also applicable to the output-only case, where $\mathbf{K}(q) = \mathbf{O}$ and the factorization applies to $\mathbf{L}(q)$.

In this way, the dispersion analysis framework developed in Section 2 can be extended also to transfer function model representations, through their state-space realization. Thus, during a structural identification process, different models and different methods can be

assessed *under the same criterion* (dispersion metric). This indeed attributes a *global* character to the proposed scheme.

4. The identification experiments

4.1. Simulated structure

The proposed methodology is now applied and assessed to the parametric identification problem of the NASA Mini-Mast space truss illustrated in Figure 1. A two-input, two-output, 10th order reduced model of the structure is provided by Lew et al. (1993) and

discretized using ZOH at $T_s = 0.03\ s$ (Abdelghani et al., 1998). Table 1 illustrates the vibration modes, from where it is observed that the reduced structural system is characterized by two pairs of very closely spaced bending modes and an additional torsional one. Following the analysis of Section 2, the second mode is detected as the heaviest contributor to the stochastic vibration energy of the system, and this is further confirmed by the corresponding normalized modal error norm (Goethals and De Moor, 2002, normalization as in equation (32)), $\bar{l}_{n,\infty}$.

In order to examine its effectiveness, the dispersion analysis framework is applied to (a) the PO-MOESP
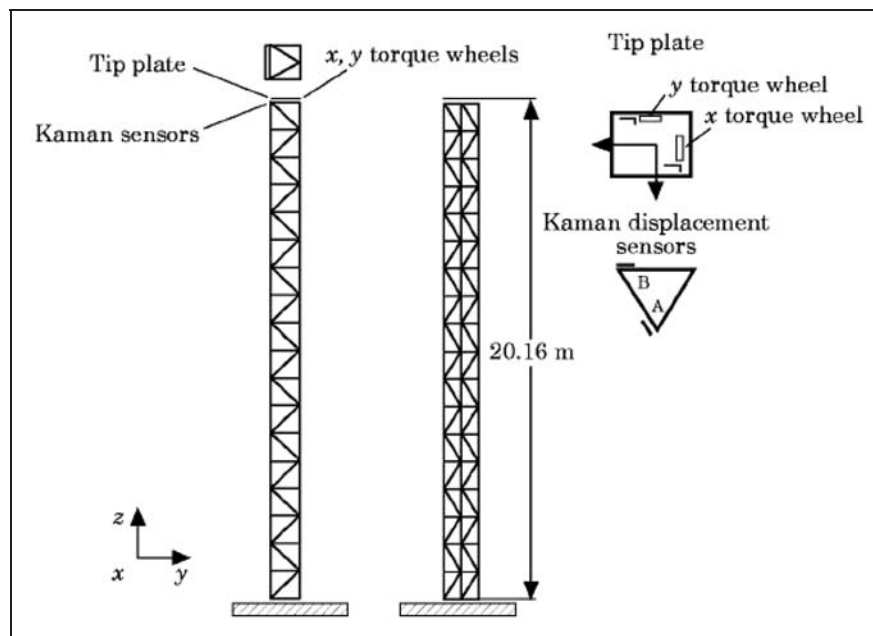

Figure 1. The NASA Mini-Mast truss structure used for the identification experiments.

Table 1. Vibration modes, modal dispersions, and modal error norms of the reduced Mini-Mast model (discrete-time, $\Sigma_{ff} = I_2$). Damping corresponds to the real part of the continuous-time eigenvalues.

Mode	Type	$f_n(Hz)$	Damping	Δ_n	$\delta_{\Delta,n,\infty}$	$\bar{\delta}_{\Delta,n,\infty}$	$\bar{l}_{n,\infty}$
1	bending	0.8008	0.09059	$\begin{bmatrix} 10.1275 & -41.0437 \\ -42.9991 & -42.8697 \end{bmatrix}$	86.0240	0.373	0.607
2	bending	0.8014	0.09066	$\begin{bmatrix} 89.4563 & 140.9371 \\ 142.8910 & 56.4842 \end{bmatrix}$	230.2774	1.000	1.000
3	torsional	4.3640	0.32907	$\begin{bmatrix} 0.1198 & -0.2438 \\ -0.2430 & 0.1235 \end{bmatrix}$	0.3665	0.002	0.021
4	bending	6.1038	0.38352	$\begin{bmatrix} 0.0480 & -0.2168 \\ -0.1897 & -0.2141 \end{bmatrix}$	0.4038	0.002	0.020
5	bending	6.1565	0.38683	$\begin{bmatrix} 0.2484 & 0.5671 \\ 0.5407 & 0.3085 \end{bmatrix}$	0.8492	0.004	0.030

subspace identification method (Verhaegen and Verdult, 2007; Verhaegen, 1994) and (b) the two-stages least squares (2SLS) method for the estimation of VARMAX models (Ljung, 1999, Chapter 10). The estimation is based on simulation data that consists of zero-mean Gaussian excitation with covariance matrix

$$\Sigma_{ff} = \begin{bmatrix} 97.9079 & -0.5314 \\ -0.5314 & 97.7487 \end{bmatrix}$$

and corresponding noise-corrupted vibration responses at 10% noise-to-signal (N/S) ratio (white measurement noise). The input–output data set is $N = 5000$ samples (150 s) long.

4.1.1. PO-MOESP identification. The number of block rows that correspond to the size of the associated Hankel matrix is chosen equal to 50 and model orders that vary from 10 to 30 are estimated. Both the frequency stabilization diagram (Figure 2) and the variance accounted for (VAF) values (Verhaegen and Verdult, 2007, Chapter 10) (Figure 3) suggest models of order $n = 13$ or higher. Accordingly, a state-space model order $n = 14$ is selected. Table 2 displays the dispersion metrics of the selected model, along with the

modal error norms. The dispersion metrics indicate the presence of five structural modes and of two spurious modes, one of which is stabilized at low orders, with negligible dispersions and modal error norms.

4.1.2. 2SLS identification. According to Fassois (2001) a fifth order, two dimensional VARMAX model would be sufficient for the description of structural dynamics. Yet, it is well-known that under noise-corrupted data a certain degree of overdetermination to the estimated transfer functions is unavoidable, so VARMAX $(k, k + 1, k, 0)$ models were estimated for $k = 5 - 25$. The estimation results are displayed in Figures 4 and 5, where the stabilization diagram and the BIC criterion are shown, respectively. Although the BIC qualifies VARMAX(7,8,7,0) as the best candidate, structural frequencies are stabilized at a considerably higher order, leading to the final selection of VARMAX(19,20,19,0) as the most appropriate model. It should be noted that the stabilization diagram in this case is more ambiguous than the previous one (Figure 2). The dispersion metrics shown in Table 3 have correctly identified five modes as structural and the rest of the modes of the VARMAX models as spurious.
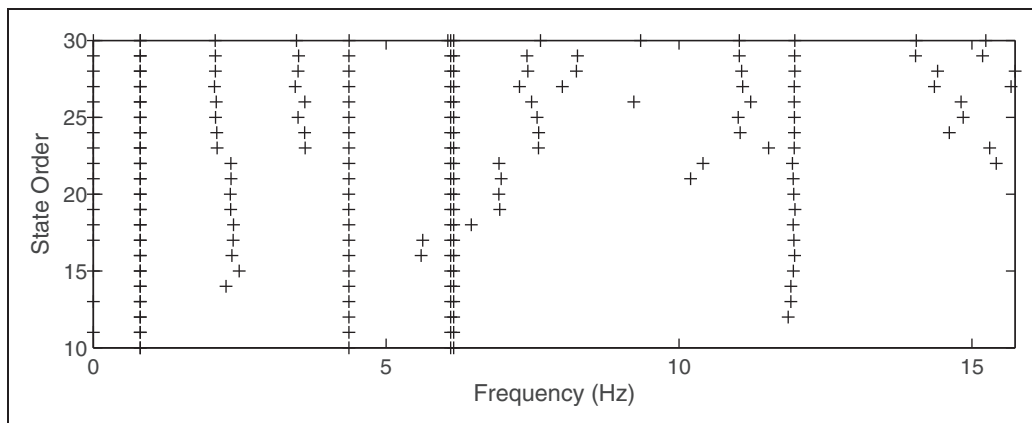

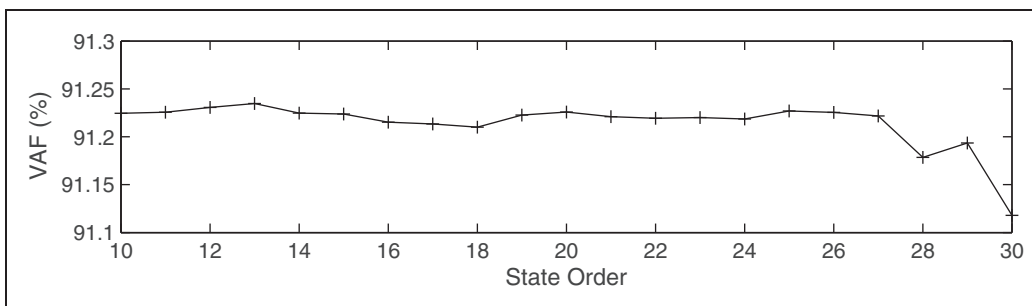**Figure 2.** Frequency stabilization diagram (Mini-Mast structure; PO-MOESP; 10% added white measurement noise).

Figure 3. VAF values. (Mini-Mast structure; PO-MOESP; 10% added white measurement noise).

Table 2. Estimated vibration modes, modal dispersions and modal error norms (Mini-Mast structure; PO-MOESP; 10% added white measurement noise). Damping corresponds to the real part of the continuous-time eigenvalues. Structural modes are in boldface.

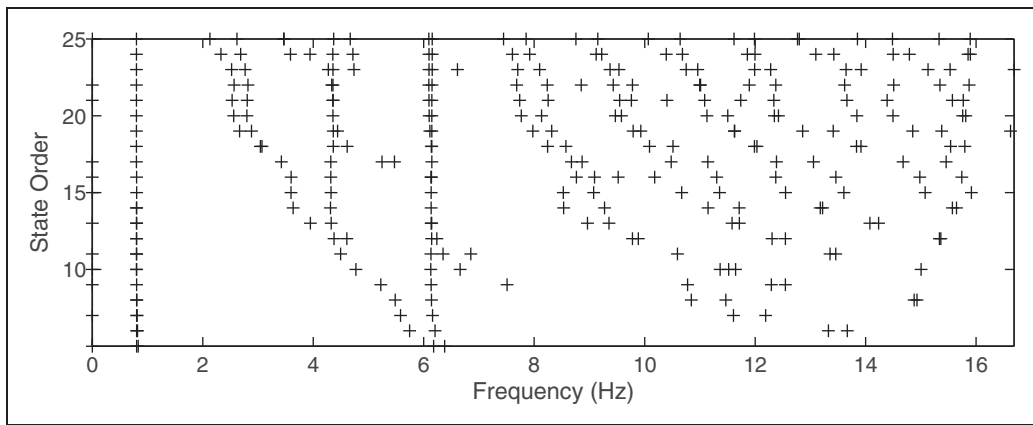| Mode	f_n (Hz)	Damping	$\delta_{\Delta,n,2}$	$\delta_{\Delta,n,\infty}$	$\bar{\delta}_{\Delta,n,2}$	$\bar{\delta}_{\Delta,n,\infty}$	$\bar{l}_{n,\infty}$
1	**0.8008**	**0.08873**	**84.6840**	**97.3838**	**0.372**	**0.388**	**0.618**
2	**0.8016**	**0.09061**	**227.5447**	**250.8549**	**1.000**	**1.000**	**1.000**
3	2.2657	0.83189	0.0753	0.0868	0.000	0.000	0.001
4	**4.3641**	**0.32235**	**0.3461**	**0.3655**	**0.002**	**0.001**	**0.021**
5	**6.1002**	**0.40026**	**0.6935**	**0.7428**	**0.003**	**0.003**	**0.019**
6	**6.1525**	**0.37787**	**1.8096**	**1.9646**	**0.008**	**0.008**	**0.029**
7	11.9081	0.76971	0.0322	0.0408	0.000	0.000	0.001

Figure 4. Frequency stabilization diagram (Mini-Mast structure; 2SLS; 10% added white measurement noise).
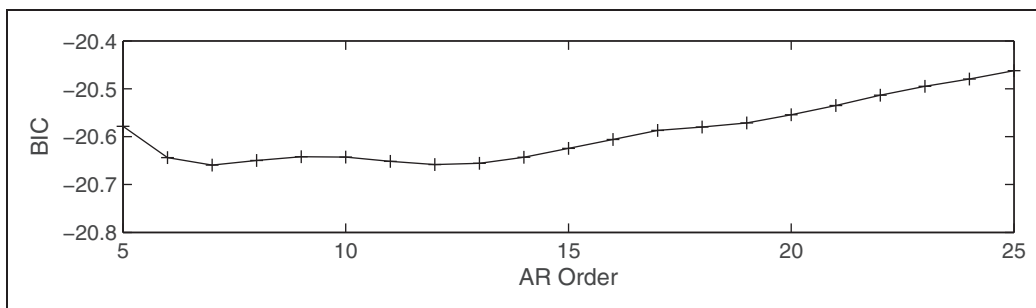

Figure 5. BIC criterion. (Mini-Mast structure; 2SLS; 10% added white measurement noise).

4.1.3. Remarks. In comparison to Table 2, the dispersion metrics for the first mode of the VARMAX model result somehow amplified while for the rest of the structural modes suppressed. While the problem of estimating the vibration modes of the Mini-Mast structure is indeed very challenging, since the three trailing modes are inherently characterized by very small contribution (see the dispersion metrics in Table 1), PO-MOESP results in better performance than 2SLS, as the estimated dispersion metrics of the first two dominant modes are more close to the true ones.

4.2. Experimental structure

In this section the proposed dispersion analysis framework is applied to the structural identification problem of a suspended steel subframe flexible structure, which is described in Abdelghani et al. (1997). The data set

Table 3. Estimated vibration modes, modal dispersions and modal error norms (Mini-Mast structure; 2SLS; 10% added white measurement noise). Damping corresponds to the real part of the continuous-time eigenvalues. Structural modes are in boldface.

| Mode	f_n (Hz)	Damping	$\delta_{\Delta,n,2}$	$\delta_{\Delta,n,\infty}$	$\bar{\delta}_{\Delta,n,2}$	$\bar{\delta}_{\Delta,n,\infty}$	$\bar{l}_{n,\infty}$
1	**0.8012**	**0.08905**	**196.2879**	**211.0292**	**0.607**	**0.516**	**0.737**
2	**0.8015**	**0.09067**	**323.6243**	**408.8576**	**1.000**	**1.000**	**1.000**
3	2.2675	3.29703	0.2058	0.2851	0.000	0.000	0.000
4	2.8817	2.09023	0.1732	0.1888	0.000	0.000	0.000
5	**4.3644**	**0.54041**	**0.4839**	**0.5073**	**0.001**	**0.001**	**0.010**
6	4.4403	2.50566	0.1056	0.1322	0.000	0.000	0.000
7	**6.1136**	**0.56398**	**0.8794**	**1.0762**	**0.003**	**0.003**	**0.012**
8	**6.1476**	**0.43014**	**2.0536**	**2.4349**	**0.006**	**0.006**	**0.022**
9	7.9768	2.64781	0.0828	0.1057	0.000	0.000	0.001
10	8.3173	3.12301	0.1556	0.2062	0.000	0.001	0.001
11	9.7927	2.27132	0.0297	0.0371	0.000	0.000	0.000
12	9.9316	4.19184	0.0761	0.0613	0.000	0.000	0.001
13	11.6239	2.60061	0.1178	0.1453	0.000	0.000	0.001
14	11.6302	3.66401	0.1361	0.1121	0.000	0.000	0.001
15	12.8610	4.64306	0.0898	0.0926	0.000	0.000	0.001
16	13.4140	2.98142	0.0758	0.0952	0.000	0.000	0.000
17	14.8540	2.94889	0.0396	0.0398	0.000	0.000	0.001
18	15.3772	4.38050	0.0778	0.1089	0.000	0.000	0.000
19	16.6239	5.36768	0.0959	0.1024	0.000	0.000	0.001
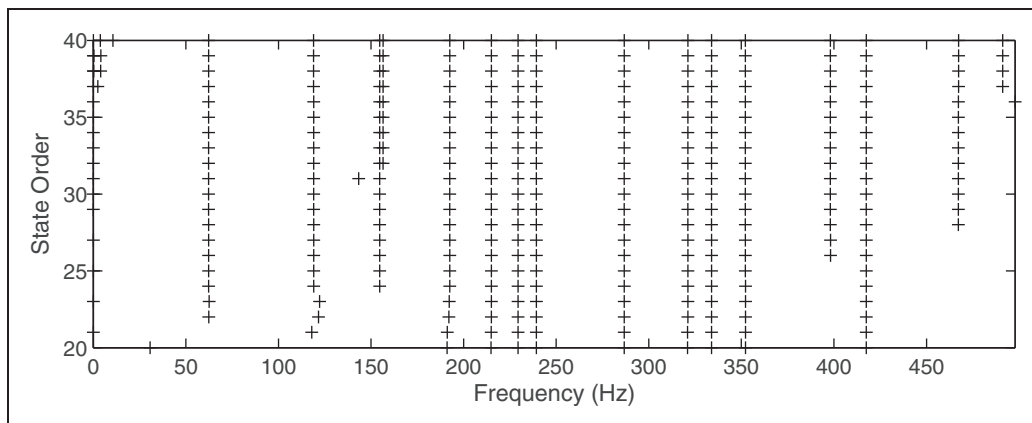
Figure 6. Frequency stabilization diagram (Steel subframe structure; PO-MOESP).

(8523 samples per channel, sampling frequency $F_s = 1024$ Hz) is available thanks to the SISTA Identification Database (De Moor, n.d.) and it consists of 2 force input signals and 28 vibration acceleration responses around the structure. The input–output data set used for the identification tasks consists of the first 4000 samples of both the input channels and of six output channels (node numbers 1, 2, 12, 13, 16, and 26). The same methods as before are utilized to the estimation of the structure. It is noted that in order to be consistent to previously published results for the same structure (Abdelghani et al., 1997), the analysis concentrated to modes within the [25 512] Hz frequency band and for damping between 0.0001% and 50%.

4.2.1. PO-MOESP identification. As nonparametric analysis shows the existence of at least 10 to 12 modes (Abdelghani et al., 1997), the number of block rows that correspond to the size of the associated Hankel matrix is chosen to be equal to 70 and model orders that vary from 20 to 40 are estimated. The results are displayed in Figures 6 and 7, again in the form of
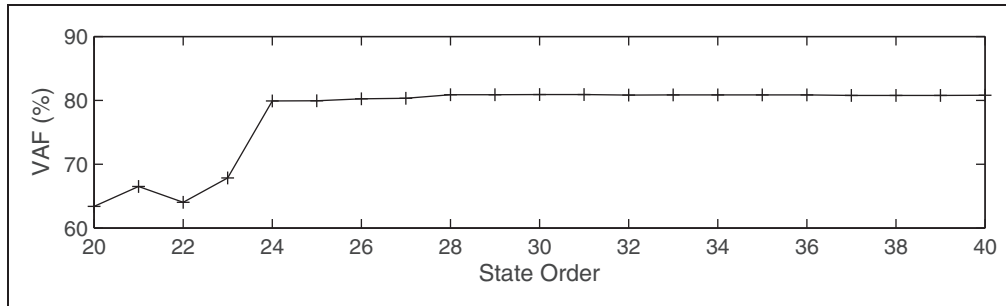
Figure 7. BIC criterion. (Steel subframe structure; PO-MOESP.)

Table 4. Estimated vibration modes, modal dispersions, and modal error norms (Steel subframe structure; PO-MOESP). Only modes within the [25 512] Hz frequency band and for damping between 0.0001% and 50% are shown. Modes identified as structural are in boldface.

Mode	f_n (Hz)	Damping	$\delta_{\Delta,n,2}$	$\delta_{\Delta,n,\infty}$	$\bar{\delta}_{\Delta,n,2}$	$\bar{\delta}_{\Delta,n,\infty}$	$\bar{I}_{n,\infty}$
1	**62.261**	**0.656**	**64.7930**	**106.7569**	**0.1850**	**0.1603**	**0.0163**
2	**119.002**	**0.166**	**31.1569**	**49.4391**	**0.0890**	**0.0743**	**0.0371**
3	**154.668**	**0.085**	**16.3832**	**30.3043**	**0.0468**	**0.0455**	**0.0063**
4	156.534	0.198	0.8083	1.3510	0.0023	0.0020	**0.0007**
5	**192.486**	**0.260**	**26.1539**	**43.2756**	**0.0747**	**0.0065**	**0.0087**
6	**214.975**	**0.118**	**57.1020**	**83.6428**	**0.1630**	**0.1256**	**0.0005**
7	**229.442**	**0.158**	**350.2189**	**665.8102**	**1.0000**	**1.0000**	**0.0142**
8	**239.335**	**0.264**	**135.4418**	**228.1775**	**0.3867**	**0.3427**	**0.0176**
9	**286.755**	**0.183**	**112.1656**	**222.7348**	**0.3203**	**0.3345**	**0.0157**
10	**321.134**	**0.151**	**43.3165**	**67.6552**	**0.1237**	**0.1016**	**0.0072**
11	**333.946**	**0.160**	**165.3042**	**261.0006**	**0.4721**	**0.3920**	**0.0154**
12	**352.204**	**0.248**	**82.5539**	**136.9826**	**0.2357**	**0.2057**	**0.0196**
13	**398.072**	**0.153**	**11.1431**	**20.0276**	**0.0318**	**0.0301**	**0.2510**
14	**417.465**	**0.105**	**143.6546**	**241.0659**	**0.4102**	**0.3621**	**1.0000**
15	**467.308**	**0.206**	**10.1207**	**16.7363**	**0.0289**	**0.0251**	**0.2000**
16	491.142	0.271	0.6115	0.9594	0.0017	0.0014	0.0097

frequency stabilization and VAF diagrams, respectively. From the latter figure a model of order $n = 30$ is suggested but, as can be seen in Figure 6, some modes are stabilized in higher orders. This leads to the selection of $n = 37$ as the appropriate state order.

Table 4 displays the dispersion metrics and the modal error norms of the selected model. It is evident that the stochastic vibration energy is dispersed among many modes and that most of the energy is concentrated at the [200 350] Hz band, while an additional mode (the 14th one, at 417.465 Hz) also retains high energy content. Two modes, the 4th and the 16th, are suspicious due to their very low dispersion metrics. Moreover, a clear disagreement between the modal dispersion metrics and the modal error norms is observed, as the latter indicate that most of the energy is

concentrated at the [400 470] Hz band. This result is, however, contradictory to the indications from the nonparametric estimates, which comply to the dispersion analysis ones.

4.2.2. 2SLS identification. The results of the estimation of VARMAX($k, k+1, k, 0$) models for $k = 4 - 15$ are depicted in Figures 8 and 9. Although the BIC criterion attains its minimum for $k = 8$, the VARMAX(10,11,10,0) mode was finally selected, since it seems that above this order the frequencies start to stabilize (Figure 8). Thus, again overdetermination proves unavoidable. As illustrated in Table 5, 15 vibration modes were identified here as well, while dispersion analysis discarded 8 more as spurious. Again, disagreement with the modal error norm is obvious.
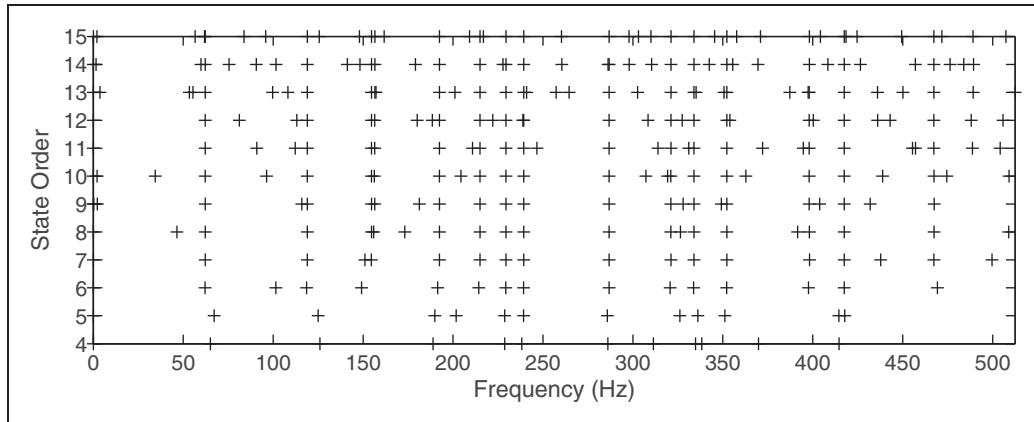
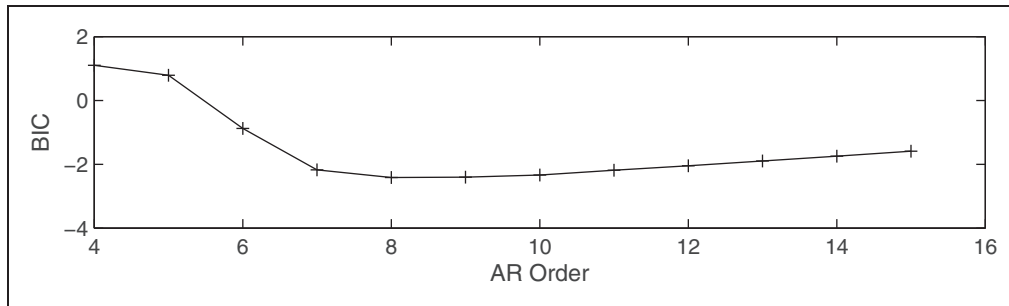**Figure 8.** Frequency stabilization diagram (Steel subframe structure; 2SLS).

Figure 9. BIC criterion (Steel subframe structure; 2SLS).

Table 5. Estimated vibration modes, modal dispersions and modal error norms (Steel subframe structure; 2SLS). Only modes within the [25 512]Hz frequency band and for damping between 0.0001% and 50% are shown. Modes identified as structural are in boldface.

Mode	f_n (Hz)	Damping	$\delta_{\Delta,n,2}$	$\delta_{\Delta,n,\infty}$	$\bar{\delta}_{\Delta,n,2}$	$\bar{\delta}_{\Delta,n,\infty}$	$\bar{l}_{n,\infty}$
1	**62.250**	**0.655**	**39.4391**	**60.5168**	**0.0239**	**0.0315**	**0.4439**
2	96.373	43.300	0.5276	0.5420	0.0003	0.0003	0.0018
3	**119.006**	**0.170**	**318.0198**	**347.2865**	**0.1925**	**0.1806**	**0.4320**
4	**154.655**	**0.089**	**25.8525**	**28.9100**	**0.0157**	**0.0150**	**0.4843**
5	156.309	0.444	2.9007	3.3818	0.0018	0.0018	0.0182
6	**192.480**	**0.257**	**46.2405**	**53.2194**	**0.0280**	**0.0277**	**0.0005**
7	204.435	20.427	2.2038	2.3542	0.0013	0.0012	1.0000
8	**214.976**	**0.128**	**246.2037**	**275.4982**	**0.1490**	**0.1433**	**0.0002**
9	229.445	0.155	1651.8599	1922.6608	1.0000	1.0000	0.1869
10	**239.328**	**0.259**	**130.6726**	**229.2881**	**0.0791**	**0.1193**	**0.5156**
11	**286.749**	**0.185**	**109.3640**	**200.7942**	**0.0662**	**0.1044**	**0.7421**
12	307.205	15.356	0.8830	1.7051	0.0005	0.0009	0.6274
13	319.253	10.115	1.1054	1.2147	0.0007	0.0006	0.4440
14	**321.128**	**0.159**	**23.5248**	**34.5900**	**0.0142**	**0.0180**	**0.0002**
15	**333.951**	**0.156**	**223.2171**	**252.8298**	**0.1351**	**0.1315**	**0.8450**
16	**352.215**	**0.248**	**39.2654**	**75.0049**	**0.0238**	**0.0390**	**0.3062**
17	362.852	10.066	4.3039	4.6083	0.0026	0.0024	0.1511

(continued)

Table 5. Continued.

Mode	f_n (Hz)	Damping	$\delta_{\Delta,n,2}$	$\delta_{\Delta,n,\infty}$	$\bar{\delta}_{\Delta,n,2}$	$\bar{\delta}_{\Delta,n,\infty}$	$\bar{l}_{n,\infty}$
18	**398.011**	**0.148**	**25.3417**	**32.4184**	**0.0153**	**0.0169**	**0.0004**
19	**417.490**	**0.107**	**161.3172**	**201.4029**	**0.0977**	**0.1048**	**0.0003**
20	438.850	8.852	1.0448	1.4039	0.0006	0.0010	0.0141
21	**467.418**	**0.212**	**39.3773**	**42.8258**	**0.0238**	**0.0223**	**0.5984**
22	474.527	11.971	11.7106	19.7710	0.0071	0.0103	0.0026
23	509.158	1.688	3.63816	3.6901	0.0020	0.0019	0.0007

4.2.3. Remarks. Just as in the Mini-Mast space truss, the PO-MOESP method is characterized by greater accuracy and modest overdetermination, while the 2SLS expectedly requires higher orders, in order to capture the structural dynamics. Regarding the dispersion metrics, their performance is similar in both cases, qualifying the same natural frequency (at about 229 Hz) as the dominant one. However, both the $l_{n,2}$ and $l_{n,\infty}$ metrics of the 2SLS result considerably higher than the corresponding values of the PO-MOESP.

5. Conclusions

The aim of this study was to present a novel framework for model assessment in structural identification, emphasizing the crucial issue of order estimation. To this end, the state-space model representation was used and a dispersion analysis framework was formulated on the basis of a modal decomposition of the output's covariance matrix. Correspondingly, dispersion metrics were defined in order to quantitatively assess the contribution of a specific structural mode to the total stochastic vibration energy under wideband excitation. It was then shown how these metrics can be implemented in an inverse framework for the validation of the state order. Consequently, the method was generalized to cover transfer function model representations as well. Thus, a global characterization was attributed, in the sense that the proposed method can be be used to validate any model-based identification process, or compare diverse methods under a common tool.

The application of the method to well-known simulated and experimental structural identification problems produced encouraging results and revealed the usability of the dispersion metrics to both the extraction of structural modes and the determination of spurious ones, which in many cases are stabilized in the relative diagrams. However, further research is required and some critical issues, like the thresholds under which a mode is characterized as spurious, are under ongoing investigation. Moreover, the application of the method to operational modal analysis and output-only identification is of immediate concern.

In this respect, it would be very interesting to explore the possibility of integrating the proposed method to operations such as the clearing of frequency stabilization diagrams and the automated modal analysis.

Note

1. Throughout the text, parentheses refer to continuous quantities, and brackets refer to discrete quantities. Bold symbols designate matrices and vectors. Hats notate estimators/estimates, and $E\{\cdot\}$ denotes expectation.

References

Abdelghani M, Chou CT and Verhaegen M (1997) Using subspace methods in the identification and modal analysis of structures. In: *Proceedings of the 15th international modal analysis conference, IMAC-XV*, Orlando, FL.

Abdelghani M, Verhaegen M, Van Overschee P and De Moor B (1998) Comparison study of subspace identification methods applied to flexible structures. *Mechanical Systems and Signal Processing* 12(5): 679–692.

Andersen P (1997) *Identification of civil engineering structures using vector ARMA models*. Ph.D. thesis, Aalborg University, Department of Building Technology and Structural Engineering, Aalborg, Denmark.

Antonacci E, De Stefano A, Gattulli V, Lepidi M and Matta E (2012) Comparative study of vibration-based parametric identification techniques for a three-dimensional frame structure. *Structural Control and Health Monitoring* 19(5): 579–608.

Bayraktar A, Altunişik AC, Sevim B and Türker T (2011) Seismic response of a historical masonry minaret using a finite element model updated with operational modal testing. *Journal of Vibration and Control* 17(1): 129–149.

Box GEP, Jenkins GM and Reinsel GC (2008) *Time Series Analysis, Forecasting and Control*, 4th edition. Upper Saddle River, NJ: Prentice Hall.

Brockwell PJ and Davis RA (2002) *Introduction to Time Series and Forecasting*, 2nd edition. New York: Springer-Verlag.

Caicedo JM (2011) Practical guidelines for the natural excitation technique (NExT) and the eigensystem realization algorithm (ERA) for modal identification using ambient vibration. *Experimental Techniques* 35(4): 52–58.

De Korte RBC (2009) *Subspace-based identification techniques for a "smart" wind turbine rotor blade: A study towards adaptive data-driven control*. Master's thesis, TU Delft, Delft, The Netherlands.

De Moor BLR (n.d.) DaISy: Database for the Identification of Systems. Available at: http://homes.esat.kuleuven.be/∼smc/daisy/(accessed 28 March 2013) [Used dataset: Experiment on a Steel Subframe Flexible structure, section Mechanical Systems, 96–013.].

Dertimanis VK and Koulocheris DV (2008) Identification of vehicle suspensions' faults from multichannel excitation and vibration response measurements. In: *Proceedings of the 3rd IC-SCCE conference*, Athens, Greece.

Dertimanis VK and Koulocheris DV (2009) On the state-space realization of vector autoregressive structures: An assessment. In: *Proceedings of the 6th ICINCO Conference*, Milan, Italy: INSTICC.

Dertimanis VK and Koulocheris DV (2011) *VaR based State-Space Structures: Realization, Statistics and Spectral Analysis* (*Lecture Notes in Electrical Engineering*, Vol. 85). Berlin: Springer, pp. 301–315.

Dertimanis VK, Koulocheris DV, Spitas V and Spitas C (2012) State-space realizations of multivariate time-series with application to the subspace estimation of vehicle dynamics. In: *Proceedings of the 5th IC-SCCE conference*, Athens, Greece.

Fadali MS (2009) *Digital Control Engineering: Analysis and Design*. Waltham, MD: Academic Press.

Farrar CR and Lieven NAJ (2007) Damage prognosis: The future of structural health monitoring. *Philosophical Transactions of the Royal Society* 365(1851): 623–632.

Farrar CR and Worden K (2006) An introduction to structural health monitoring. *Philosophical Transactions of the Royal Society* 365(1851): 303–315.

Fassois SD (2001) MIMO LMS-ARMAX identification of vibrating structures—Part I: The method. *Mechanical Systems and Signal Processing* 15(4): 723–735.

Florakis A, Fassois SD and Hemez FM (2001) MIMO LMS-ARMAX identification of vibrating structures—Part II: A critical assessment. *Mechanical Systems and Signal Processing* 15(4): 737–758.

Goethals I and De Moor B (2002) Model reduction and energy analysis as a tool to detect spurious modes. In: *Proceedings of the 2002 international conference on noise and vibration engineering, ISMA*, Leuven, Belgium.

Hannan EJ (1976) The identification and parameterization of ARMAX and state space forms. *Econometrica* 44(4): 713–723.

Juang JN and Pappa RS (1985) An eigensystem realization algorithm for modal parameter identification and model reduction. *Journal of Guidance, Control, and Dynamics* 8(5): 620–627.

Kailath T, Sayed AH and Hassibi B (2000) *Linear Estimation*, 3rd edition. Upper Saddle River, NJ: Prentice Hall.

Katayama T (2005) *Subspace Methods for System Identification*. Berlin: Springer.

Koulocheris DV, Dertimanis VK and Spentzas CN (2008) Parametric identification of vehicle structural characteristics. *Forschung im Ingenieurwesen* 72(1): 39–51.

Landau ID and Zito G (2006) *Digital Control Systems: Design, Identification and Implementation*. London: Springer.

Larbi N and Lardies J (2000) Experimental modal analysis of a structure excited by a random force. *Mechanical Systems and Signal Processing* 14(2): 181–192.

Lardies J (2008) Relationship between state-space and ARMAV approaches to modal parameter identification. *Mechanical Systems and Signal Processing* 22(3): 611–616.

Lee JE and Fassois SD (1993) On the problem of stochastic experimental modal analysis based on multiple-excitation multiple-response data—Part I: Dispersion analysis of continuous-time structural systems. *Journal of Sound and Vibration* 161(1): 33–56.

Lee JE and Lee BR (2001) Relative importance of vibrational modes in random vibration. In: *Proceedings of the 19th International modal analysis conference, IMAC-XIX*, Orlando, FL.

Lew JS, Juang JN and Longman RW (1993) Comparison Of Several System Identification Methods For Flexible Structures. *Journal of Sound and Vibration* 167(3): 461–480.

Ljung L (1999) *System Identification: Theory for the User*, 2nd edition. Upper Saddle River, NJ: Prentice Hall.

Loh CH, Weng JH, Chen CH and Lu KC (2013) System identification of mid-story isolation building using both ambient and earthquake response data. *Structural Control and Health Monitoring* 20(2): 19–35.

Lütkepohl H (2005) *New Introduction to Multiple Time Series Analysis*. Berlin: Springer.

Meyer CD (2000) *Matrix Analysis and Applied Linear Algebra*. Philadelphia, PA: Society for Industrial and Applied Mathematics.

Morassi A and Vestroni F (2008) *Dynamic Methods for Damage Detection in Structures*, (CISM Courses and Lectures). Vol. 499, New York: Springer.

Papakos V and Fassois SD (2003) Multichannel identification of aircraft skeleton structures under unobservable excitations: A vector AR/ARMA framework. *Mechanical Systems and Signal Processing* 17(6): 1271–1290.

Petsounis KA and Fassois SD (2001) Parametric time-domain methods for the identification of vibrating structures—a critical comparison and assessment. *Mechanical Systems and Signal Processing* 15(6): 1031–1060.

Ren WX and Zong ZH (2004) Output-only modal parameter identification of civil engineering structures. *Structural Engineering and Mechanics* 17(3–4): 429–444.

Reynders E (2012) System identification methods for (operational) modal analysis: Review and comparison. *Archives of Computational Methods in Engineering* 19(1): 51–124.

Reynders E and De Roeck G (2008) Reference-based combined deterministic-stochastic subspace identification for

experimental and operational modal analysis. *Mechanical Systems and Signal Processing* 22(3): 617–637.

Reynders E, Houbrechts J and De Roeck G (2012) Fully automated (operational) modal analysis. *Mechanical Systems and Signal Processing* 29: 228–250.

Van Der Auweraer H and Peeters B (2004) Discriminating physical poles from mathematical poles in high order systems: Use and automation of the stabilization diagram. In: *Proceedings of the 21st IEEE instrumentation and measurement technology conference*, Como, Italy.

Verhaegen M (1994) Identification of the deterministic part of MIMO state space models given in innovations form from input–output data. *Automatica* 30(1): 61–74.

Verhaegen M and Verdult V (2007) *Filtering and System Identification: A Least Squares Approach*. Cambridge: Cambridge University Press.

Yang QJ, Zhang PQ, Li CQ and Wu XP (1994) A system theory approach to multi-input multi-output modal parameters identification methods. *Mechanical Systems and Signal Processing* 8(2): 159–174.